CHEMISTRY
A EUROPEAN JOURNAL

DOI: 10.1002/chem.200601166

# Exceptional Affinity of Nanostructured Organic–Inorganic Hybrid Materials towards Dioxygen: Confinement Effect of Copper Complexes

**Stéphane Brandès,[a] Gabriel David,[a] Clément Suspène,[a] Robert J. P. Corriu,[b] and Roger Guilard*[a]**

**Abstract:** We report the exceptional reactivity towards dioxygen of a nanostructured organic–inorganic hybrid material due to the confinement of copper cyclam within a silica matrix. The key step is the metalation reaction of the ligand, which can occur before or after xerogel formation through the sol–gel process. The incorporation of a $Cu^{II}$ center into the material after xerogel formation leads to a bridged $Cu^{I}$/$Cu^{II}$ mixed-valence dinuclear species. This complex exhibits a very high affinity towards dioxygen, attributable to auto-organization of the active species in the solid. The remarkable properties of these copper complexes in the silica matrix demonstrate a high cooperative effect for $O_2$ adsorption; this is induced by close confinement of the two copper ions leading to *end-on* $\mu$-$\eta^1$:$\eta^1$-peroxodicopper(II) complexes. The anisotropic packing of the tetraazamacrocycle in a lamellar structure induces an exceptional reactivity of these copper complexes. We show for the first time that the organic–inorganic environment of copper complexes in a silica matrix fully model the protecting role of protein in metalloenzymes. For the first time an oxygenated dicopper(II) complex can be isolated in a stable form at room temperature, and the reduced $Cu_2^{I,I}$ species can be regenerated after several adsorption–desorption cycles. These data also demonstrate that the coordination scheme and reactivity of the copper cyclams within the solid are quite different from that observed in solution.

**Keywords:** copper · dioxygen binding · organic–inorganic hybrid composites · sol–gel processes · tetraazamacrocycles

## Introduction

Much effort has been directed towards modeling the reactions of copper enzymes with dioxygen[1–3] in order to elucidate the mechanism of dioxygen activation by copper monooxygenases, and to develop efficient catalytic systems for the selective oxidation of organic substrates by dioxygen.[4–8] A range of copper–dioxygen complexes,[1–10] containing $\mu$-$\eta^2$:$\eta^2$-peroxodicopper(II) and bis($\mu$-oxo)dicopper(III) moieties, has been studied extensively, since these binuclear metal sites have been proposed as models of the reactive intermediates at the active sites of copper monooxygenases. The understanding of how synthetic model systems and copper proteins utilize dioxygen to oxidize substrates is a timely and important research topic. Appropriate tripodal ligands[6,9,10] have frequently been designed and used in bioinorganic studies as their coordination schemes are similar to those at the active sites of metalloenzymes, and they allow tuning of the steric and electronic properties of the metal center. These systems have been considered as structural or functional models of copper-containing enzymes such as hemocyanin,[11,12] tyrosinase,[13] galactose oxidase,[14] superoxide dismutase and ascorbate oxidase, among others.[2] Apart from hemocyanin, these copper metalloenzymes and their designed functional models lead to dioxygen activation, which has been the topic of many studies.[15,16] In order to build new types of dioxygen binding models and smart materials able to reversibly carry dioxygen, new complexes have been synthesized with mainly tri- or tetradentate tripodal architectures.[17–22] However, these remarkable coordination properties have not been explored to synthesize materials able to undergo similar reactivities.

Nanostructured organic–inorganic hybrid materials based on silica have attracted considerable attention during the

[a] Dr. S. Brandès, Dr. G. David, C. Suspène, Prof. Dr. R. Guilard
LIMSAG, UMR 5633, Université de Bourgogne
UFR Sciences et Techniques
9 avenue Alain Savary, BP 47870, 21078 Dijon Cedex (France)
Fax: (+33) 380-396117
E-mail: roger.guilard@u-bourgogne.fr

[b] Prof. Dr. R. J. P. Corriu
LCMOS, UMR 5637 CNRS, Université de Montpellier II
Sciences et Techniques du Languedoc, Place E. Bataillon
34095 Montpellier Cedex 5 (France)

last decade.[23,24] The sol–gel chemistry allows the preparation of hybrid organic–inorganic materials called polysilsesquioxanes[25,26] in which the organic fragments are located within a silica framework. They are obtained by the hydrolysis and polycondensation of bis- or poly(trialkoxysilyl) organic precursors,[25,26] leading to materials in which the organic fragments are integrated into the silica by covalent bonds. It has also been proven that a kinetically controlled hydrolysis[25] and organization of the organic units occurs at both the nanometric and micrometric scale due to van der Waals interactions, hydrogen bonds, and coulombian interactions. Such interactions lead to nano-organization of the molecular units over a short[24,27] or a long range.[28–31]

This class of organic-inorganic hybrid material is of great interest for a broad field of investigation, since the properties can be modified by changing the nature of the bridging organic groups. Moreover, these nanostructured materials can be prepared by incorporating many different organic chelates and complexes into the framework.[32–41] Finally, increased stability of the immobilized complexes within the material is expected when compared to the isolated units.

Therefore, application of the chelate-functionalized silicas can lead to promising materials in many areas such as catalysis;[42] metal-ion separation processes, especially for transition metals,[43–45] heavy metals[46–48] and actinides;[36] as well as chemical[49] and optical sensors.[50,51] Despite the growing interest in functionalized sol–gel materials, only a few examples are known for gas separation through the formation of chemical bonds between gas molecules and coordination complexes immobilized in an inorganic matrix by way of chemisorption,[39,40,52,53] and their use as gas sensors is still scarce. Mainly optical $O_2$ sensors based on fluorescence quenching have been studied,[50,51,54–57] but a lack of selectivity[58] is generally observed when there is no covalent binding of the gas molecule to the active species.

An outstanding challenge in the study of organic–inorganic hybrid systems is the development of materials with unexpected properties when examining the organosilylated precursor, because these properties can be induced by the nano-organization of the active species into the inorganic framework. Thus, unusual adsorption properties may arise by incorporating metallo-organic units into inorganic frameworks due to the arrangement of the organic moieties, giving rise to short-range organization.[24,27] Moreover, hybrid xerogels can combine the textural and structural properties of the inorganic matrix, allowing tuning of the gas binding properties of the immobilized copper complexes. Furthermore, the incorporation of these complexes into a solid inorganic network should avoid degradation of the active species, which is a prerequisite for the regeneration of the materials after the first $O_2$ binding cycle.

With this aim, materials incorporating strong chelating agents, such as tetrazacyclotetradecane (cyclam), into their framework were prepared and their coordination chemistry towards copper(II) binding,[59–61] as well as their reactivities within the solid were explored. Cyclam[62] constitutes a useful building block for the creation of porous hybrid systems, since it results in a scaffold possessing four polycondensation directions with a central cavity able to coordinate transition-metal ions. The various topologies of the ligands lead to a wide variety of coordination modes with metal centers; examples of these are square-planar, square-pyramidal,[60,63–66] and octahedral coordination geometry, and square antiprism polyhedra,[59,67–69] depending on the number and the nature of the coordinating arms anchored to the macrocycle and the stereochemical constraints. The incorporation of tetraazamacrocycles in a material should yield stabilization of unusual metal coordination stereochemistries and reactivity of the complexes.

## Results and Discussion

Bridged polysilsesquioxanes incorporating tetra-*N*-alkylated cyclam were prepared following two different routes.[34] One involved the hydrolysis and polycondensation of copper-complexed silylated cyclam complexes (Scheme 1, route A), and the other the hydrolysis and polycondensation of silylated cyclam derivatives followed by direct incorporation of copper salts into the xerogels (Scheme 1, route B). For route B, a quantitative metalation of the xerogel with copper dichloride demonstrates that all sites are accessible in the solid matrix. The materials synthesized according to these two routes exhibit totally different reactivity: the xero-

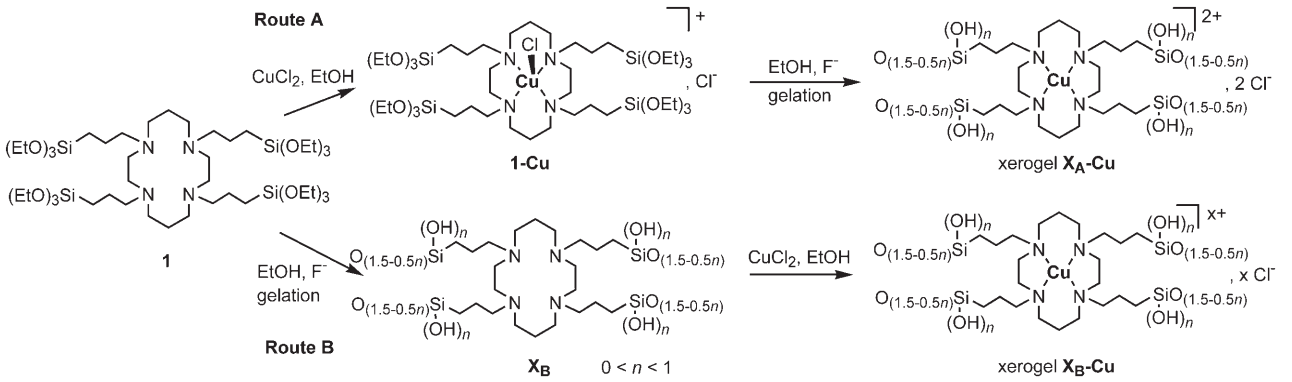


Scheme 1. Synthesis of xerogels incorporating tetraazamacrocyclic copper complexes by two different routes.

  

gel prepared according to route A is nonporous, while the xerogel from route B is micro- or mesoporous (10–50 Å) depending upon the experimental conditions.[34] The solid-state $^{29}$Si NMR spectra of nonmetalated xerogels (route B) display a pair of resonance signals[33] lying at $\delta = -58$ and $-64$ ppm; these have been assigned to the $T^2$ [C-Si(OR)-$(OSi)_2$] and $T^3$ [C-Si$(OSi)_3$] substructures, respectively, the latter predominating, which indicates that the xerogels are well polycondensed. The absence of resonance signals corresponding to Q substructures[70] between $\delta = -90$ and $-110$ ppm showed that no cleavage of Si–C bonds occurred during the sol–gel process.

Moreover, only the materials prepared from route B are able to react selectively with dioxygen rather than dinitrogen. The affinity of the copper ions in the activated solid for dioxygen is illustrated in Figure 1 for xerogels **$X_B$-Cu** prepared through route B. The addition of dioxygen at 295 K to the light brown xerogel complexed with copper ions resulted in a color change to dark green, indicating the formation of $Cu^{II}$ ions. The oxygenation reaction was monitored by adsorption experiments at 295 K under static conditions.

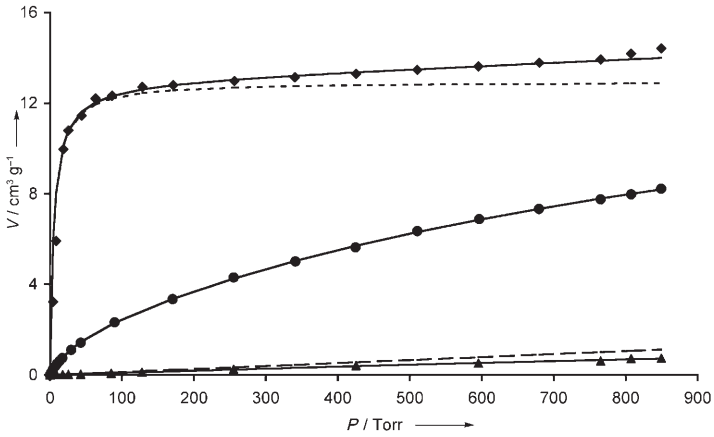


Figure 1. Experimental adsorption isotherms of ◆ $O_2$, ▲ $N_2$ and ● CO for **$X_B$-Cu** recorded at 293 K. Calculated isotherms are represented by solid lines. The dotted and dashed lines represent the first and second components respectively of the calculated isotherm for $O_2$ adsorption.

The $O_2$ adsorption isotherms were analyzed by using a multiple-site adsorption process involving a two Langmuir-type adsorption model[71–73] as has been described for cobalt–corrole xerogels,[40] and $[Co(cyclam)]^{2+}$ grafted onto silica.[52] The calculated isotherms are given in Figure 1 and Table 1 along with experimental isotherms for CO and $N_2$ adsorption. Such a model is required to describe a chemical system with heterogeneous energetic interactions. The first Langmuir-type isotherms reflect the chemisorption of dioxygen with a high energetic interaction, while the second illustrates a very low energetic interaction through a nonselective adsorption process, resulting from dissolution and diffusion of the gas into the solid material.[71–74] Furthermore, the use of only two Langmuir adsorption components to fit the experimental isotherms shows that all the sites are accessible.[40,74] Conversely, since $N_2$ is adsorbed onto the solid through a non-selective physisorption process and no coordination to the metal ions occurs, a single Langmuir adsorption model was used for this gas.

Table 1. Experimental and calculated gas adsorption data for **$X_B$-Cu** recorded at 293 K.

| | $V_{760}$[a] [cm$^3$ g$^{-1}$] | $V_1$[b] [cm$^3$ g$^{-1}$] | $(P_{1/2})_1$[c] [Torr] | $V_2$[b] [cm$^3$ g$^{-1}$] | $(P_{1/2})_2$[c] [Torr] | active sites[d] [%] |
|---|---|---|---|---|---|---|
| $O_2$ | 13.8 | 12.9 | 5.2 | 1323 | $10^6$ | 49.2 |
| CO | 7.7 | 1.7 | 37.8 | 15.9 | 1219 | 6.5 |
| $N_2$ | 0.6 | – | – | 4.9 | 4965 | 0 |

[a] Experimental volume adsorbed at 760 Torr. [b] Calculated volume for the $i^{th}$ contribution of the multisite Langmuir isotherm; $i=1$ refers to chemisorption and $i=2$ refers to nonselective physisorption by the inorganic matrix. [c] $(P_{1/2})_i = 1/K_i$. [d] Calculated from [Cu] = 1.17 mmol g$^{-1}$ and $V_1$.

The equilibrium constant relating to the $O_2$ binding affinity, $K_i$, and the adsorption capacity, $V_i$, were thus calculated by considering the combination of these two adsorption processes (see Experimental Section). These experiments clearly evidence that $O_2$ adsorption by **$X_B$-Cu** materials after an activation step involves a chemisorption process, the main adsorption contribution of the isotherm (93% considering a 2:1 Cu:$O_2$ adduct), and explain the high affinity and selectivity for $O_2$. A weak contribution of a physisorption process is also seen in the high-pressure range. The mesoporous solid **$X_B$-Cu** adsorbs 13.8 cm$^3$ g$^{-1}$ $O_2$ at 760 Torr, and the half saturation pressure ($(P_{1/2})^{O_2} = 1/K_{O_2}$) equal to 5 Torr, illustrating the very strong affinity of the material for dioxygen. The key feature of the material is the selectivity for $O_2$ adsorption compared to $N_2$. This selectivity, defined by the ratio $(P_{1/2})_2^{N_2}/(P_{1/2})_1^{O_2}$, is about 1000 and $N_2$ is only slightly adsorbed by the solid through a physisorption process and not by coordination on the metal ions. The high specific surface area observed after complexation should explain the high accessibility of the coordination sites for dioxygen. However, these results show that the large specific surface areas and porosities are not the main criteria for a large $O_2$ capacity, since the complexation of microporous or even nonporous xerogels obtained by hydrolysis of precursor **1** in mild conditions[33] have also shown a high affinity for $O_2$, but with a significantly lower percentage of active sites ($\approx$30%). Therefore there is no straightforward correlation between the porosity and the reactivity of the copper complexes towards $O_2$.

The study of this family of compounds has shown that the hybrid xerogels are very reactive towards dioxygen after an activation procedure, that is, degassing for a few hours under vacuum while heating at around 120 °C. The data also demonstrate that chemisorption is high for $O_2$, but close to zero for $N_2$, and that several adsorption–desorption cycles can occur. Finally, the percentage of active sites, calculated from the chemisorbed volume, $V_1$, and the copper concentration in the material, was close to 50% (Table 1). The for-

  

mation of a Cu–$O_2$–Cu dimer is thus assumed to occur after oxygenation of the xerogel. Moreover, the high affinity of the materials requires the following conditions:

- A metalation of the xerogel after gelation (route B),
- $CH_3OH$, EtOH or $CH_3CN$ solvents for metalation of the xerogel,
- $CuCl_2$ as the metalating agent.

No dioxygen adsorption was observed when $CuBr_2$ was used as a metalating agent or when default $CuCl_2$ (<50% with respect to the ligand concentration in the xerogel) was used. This suggests that confinement of the metal ions in the solid is not a sufficient condition to create a material highly reactive towards $O_2$, but fine tuning of the metal–metal distance and control of the coordination polyhedron of the metal ions in the solid are needed. On the other hand, for the $CuCl_2$-complexed xerogels, the selectivity for $O_2$ adsorption over CO, defined by the ratio $(P_{1/2})_1^{CO}/(P_{1/2})_1^{O_2}$, is about 7. This indicates that the materials have a high affinity for gases able to bind copper in a bidentate way (see above), and a low affinity when the gas molecule (CO) has the propensity to behave as a monodentate ligand. Moreover, the accessibility for CO adsorption is very low, since $V_1$ represents only 6.5% of the active sites. Therefore, the affinity and capacity of the copper-complexed materials demonstrate a high cooperativity effect for $O_2$ adsorption due to confinement of the two copper ions in close proximity, thus leading to a stable dimeric Cu–$O_2$–Cu complex.

The coordination polyhedra of the copper ions, their dinuclear structure, and the oxidation state of the active site were examined by X-ray absorption spectroscopy[53] to elucidate how hybrid xerogels complexed with $CuCl_2$ could reversibly bind molecular dioxygen. Difference extended X-ray absorption fine structure (EXAFS) analysis at the Cu K-edge suggest that dioxygen bridges two Cu atoms with a μ-$\eta^1$:$\eta^1$-peroxo-like core and unequal Cu···O distances. Insights into the dioxygen adduct formed in the oxygenated xerogel can be obtained from the solution chemistry of copper(I) complexes[5,7,8] or from a systematic review of X-ray crystal structures for Cu–dioxygen complexes.[4,6,75] The oxygenation of $Cu^I$ complexes can generate three types of 2:1 Cu/$O_2$ species: an end-on μ-$\eta^1$:$\eta^1$-peroxodicopper(II), a side-on μ-$\eta^2$:$\eta^2$-peroxodicopper(II) or a bis(μ-oxo)dicopper(III). The species that forms is primarily dictated by the denticity of the ligand.[6,76] In particular, oxygenation of $Cu^I$ complexes with sterically unhindered tetradendate tripodal ligands produces exclusively end-on peroxide species, whereas $Cu^I$ complexes with tridentate ligands give side-on peroxo or bis(μ-oxo) adducts. Because no dioxygen adduct from oxygenation in solution of a tetra-*N*-functionalized cyclam copper(I) complex has been characterized, we have to rely on comparisons with other tetradendate systems described in the literature. In this regard, the aliphatic tetramine ligands derived from tris(2-aminoethyl)amine (tren)[7,77] or tris(2-pyridylmethyl)-amine (tmpa)[5,78,79] can be considered as good models for the immobilized cyclams, although these are not macrocyclic derivatives. The average Cu···O distance is quite similar (1.86±0.01 Å) to the Cu–O bond lengths for copper dioxygen complexes characterized by X-ray crystallography.[4,6] The Cu···Cu internuclear distances for the oxygenated and oxygen-free xerogels ($d_{Cu-Cu}$=4.0 and 3.9 Å respectively) are significantly longer than the Cu···Cu distances in side-on peroxodicopper complexes, but rather shorter when compared to metal–metal distances for end-on $[Cu_2(\mu\text{-}\eta^1\text{:}\eta^1\text{-}O_2)]^{2+}$ peroxodicopper(II) with tmpa[78] or tren[77] tetradentate ligands. These structures have shown an end-on *trans* binding of the peroxide ion with a Cu···Cu separation of 4.36 Å for tmpa and 4.47 Å for functionalized tren. In fact, the Cu K-edge EXAFS data rule out the last two configurations. This portends a slightly distorted arrangement of the peroxo moiety, and accordingly it is more likely that oxygenation in the copper–xerogel leads to formation of an end-on μ-$\eta^1$:$\eta^1$-peroxodicopper(II) complex. In addition, the use of a tetradentate macrocycle that coordinates copper ions in a near square-planar fashion rules out formation of side-on peroxo coordination and confirms the EXAFS results, which are consistent with an end-on μ-peroxodicopper(II) species.

Thus, the signatures of the Cu K-edge EXAFS spectra for oxygenated and oxygen-free xerogels have shown that the coordination geometry of the cyclam is slightly modified during the oxygenation reaction.[53] In the oxygen-free xerogels, the Cu and Cl K-edge EXAFS spectra[53] revealed the pre-existence of $Cu^I$ sites with short Cl–Cu bonds (2.11± 0.03 Å). Before exposure to dioxygen, pentacoordinate $Cu^{II}$ sites with a longer Cu–Cl bonds (2.45±0.03 Å) are observed. Another signal at long distance (2.73±0.03 Å) was also identified, suggesting that $Cl^-$ ions could bridge mixed valence $Cu_2^{I,II}$ sites. According to the EXAFS data, the dinuclear structure is best described as a class I mixed-valent immobilized complex, with isolated $Cu^I$ and $Cu^{II}$ ions and the unpaired electron localized on the $Cu^{II}$ site with no delocalization on the two copper ions.[80–82]

The influence of the axial and equatorial donors on the electronic properties of the complexes varied as a function of their relative interactions, due in part to steric effects. Indeed, there is an inverse correlation between the in-plane and axial bond lengths, as expected on the basis of Jahn–Teller distortions[83] and the position of the d–d absorption of copper(II) complexes is indicative of the strength of the in-plane ligand field versus the axial field. The various configurations of metalated cyclam derivatives[84] are strongly dependent on alkyl substitution at the four nitrogen atoms of the macrocycle, leading to a decrease of the ligand field as evidenced by electronic and EPR spectroscopic data. Tetra-*N*-alkylated cyclam copper(II) complexes are expected to be pentacoordinated, the copper ion being significantly shifted away from the mean plane of the four nitrogen atoms[60,65] with some trigonal distortion. The electronic spectrum of copper–cyclam complex in a square-planar[85,86] or distorted-octahedral geometry[85,87] generally exhibits a quite broad absorption band between 540 and 600 nm. These two coordination geometries can be differentiated only by the molar extinction coefficients of this band.[63,64,85]

  

In contrast, the electronic properties of square-pyramidal pentacoordinated copper-cyclam complexes[63–65] result in a broader absorption at lower energy (between 620 and 720 nm) along with a relatively high $\varepsilon$ value (210 to 270 $mol^{-1}Lcm^{-1}$). Since this absorption is expected to be due primarily to the promotion of one electron from the $d_{xz,yz}$ to $d_{x^2-y^2}$ orbital, the variation in the absorption maximum represents the effect of changes in the donor properties on the energy difference between these orbitals. In contrast to square-planar and octahedral complexes, square-pyramidal complexes are not centrosymmetric, implying that the intensity of the broad band derives from the overlap of one allowed transition $^2B_1(d_{x^2-y^2})\rightarrow{}^2E(d_{xz,yz})$ and two forbidden transitions $^2B_1(d_{x^2-y^2})\rightarrow{}^2B_2(d_{xy})$ and $^2B_1(d_{x^2-y^2})\rightarrow{}^2A_1(d_{z^2})$ in a $C_{4v}$ symmetry group. The absorption values are thus in accordance with a pentacoordinated copper(II) ion in a square-pyramidal coordination geometry of the metal ion in tetra-*N*-alkylated cyclams[60,65,88] or polyamine linear complexes.[89] These are accompanied by a slight distortion of the equatorial Cu–N bonds and a rather strong in-plane ligand field strength.[63]

When the cyclam precursor **1** is immobilized in the sol–gel matrix through route B and metalated by $CuCl_2$ (**$X_B$-Cu**), a shift of the broad envelope of bands to a higher energy occurs (Figure 2) in the visible region ($\lambda_{max}=$ 740 nm), compared to the silylated precursor complex **1-Cu** in solution ($\lambda_{max}=806$ nm, $\varepsilon=199\ mol^{-1}Lcm^{-1}$ in $CH_2Cl_2$). These electronic data are fully consistent with a square-pyramidal $CuN_4X$ chromophore, and the bathochromic shift of the d–d transition is diagnostic for a significantly stronger equatorial ligand field in the material than for the corresponding **1-Cu** complex in solution.[90,91] However, for the gelated complexes, **$X_A$-Cu**, the type I configuration[63–65] of the square-pyramidal coordination polyhedra **1-Cu** is not preserved during gelation of the complex; the single band at 550 nm reflects the hexacoordination of the copper(II) ions. Once again, the sol–gel matrix imposes steric constraints that increase the equatorial ligand field of the immobilized cyclam compared to that of the analogous precursor in solution. The sol–gel matrix is thus able to stabilize a coordination geometry unlike that observed in solution.

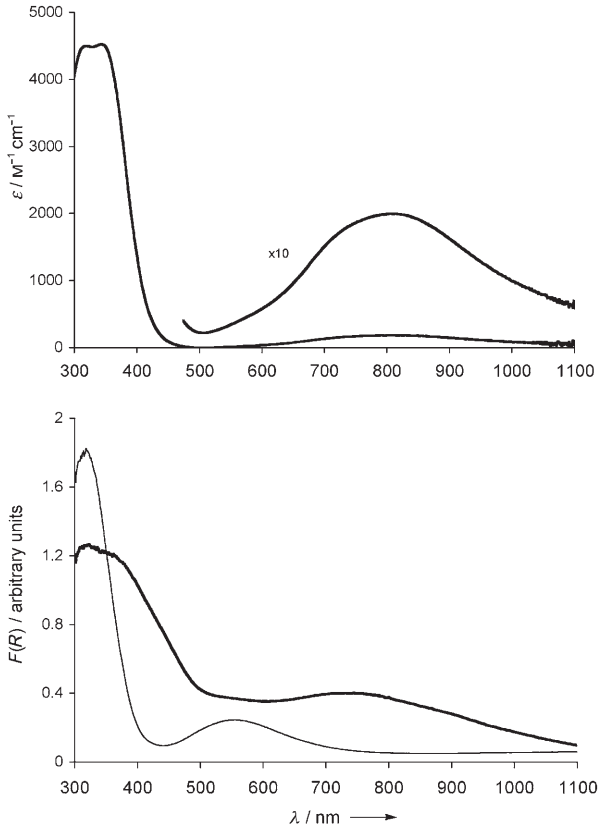


Figure 2. Absorption spectrum of **1-Cu** in $CH_2Cl_2$ (top) and solid-state diffuse-reflectance spectra of **$X_A$-Cu** (thin line) and **$X_B$-Cu** (thick line) in the visible region (bottom). Data for spectra in the bottom half are presented in Kubelka Munk units.

For **$X_B$-Cu**, a strong equatorial ligand field is revealed by the rather short in-plane copper(II)–amine EXAFS distances,[53] relative to other tetra-*N*-alkylated $Cu^{II}$–cyclam complexes analyzed by single-crystal X-ray diffraction. Indeed, the average Cu–N distance (2.02 Å) in the oxygenated and oxygen-free xerogels is significantly shorter than that for tetra-*N*-alkylated and tetra-*N*-benzylated $Cu^{II}$ complexes: these have a square-pyramidal coordination geometry in which this distance ranges from 2.08 to 2.17 Å due to pseudo-tetrahedral distortions,[60,65,92] but the distance is quite similar to other five-coordinated copper complexes with a weak axial-bond donor atom.[64,93] This result agrees well with the reactivity of the dioxygen adduct, since the relative lability of the axial dioxygen molecule is revealed by its desorption under vacuum.

Elucidation of the oxygenation mechanism in the xerogels and monitoring of any changes in the copper oxidation state during the oxygenation process should provide a better understanding of their exceptional reactivity towards dioxygen. A proposed mechanism for the reaction scheme is shown in Scheme 2. Since dioxygen is not able to coordinate to copper(II) ions, formation of the active complex requires reduction to a $Cu^I/Cu^{II}$ species in the first step of the reaction mechanism. These redox properties can be compared to the behavior of overexchanged copper–zeolite species.[94–96] Indeed, the redox chemistry of copper species within such inorganic frameworks has been well established for Cu-ZSM-5: a self-reduction pathway of copper(II) ions introduced by ion exchange into Na-ZSM-5 involving extra lattice oxygen atoms was proposed to explain this reactivity. The reduction of copper(II) to copper(I) in zeolite upon thermal treatment under vacuum has been probed by EPR studies and CO adsorption.[94,97] Moreover, the mechanism proposed by Larsen et al. implies a complex pathway involving the formation of hydroxyl radicals.[94] Therefore, in the case of the copper xerogel **$X_B$-Cu**, the reduction of copper(II) should proceed by the formation of ethoxy radicals through electronic transfer between the metal ions and the coordinated solvent molecules.

For cyclam xerogels, the EXAFS data have shown that the active species after pre-treatment by heating (393 K

  

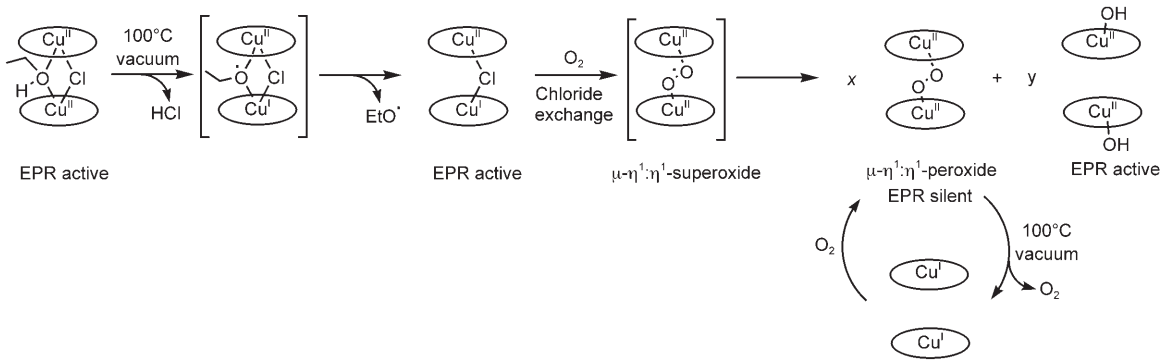


Scheme 2. Proposed mechanism for $Cu^{II}/Cu^{I}$ and dioxygen adduct formation in xerogel $\mathbf{X_B}$-**Cu**.

under vacuum under argon) are mixed valence $Cu_2^{I,II}$ species; this mixed valence system was confirmed by recording the in situ EPR spectra under argon and after exposure of the sample to dioxygen. Examination of the EPR spectra (Figure 3) confirms that the unpaired electron of the mixed

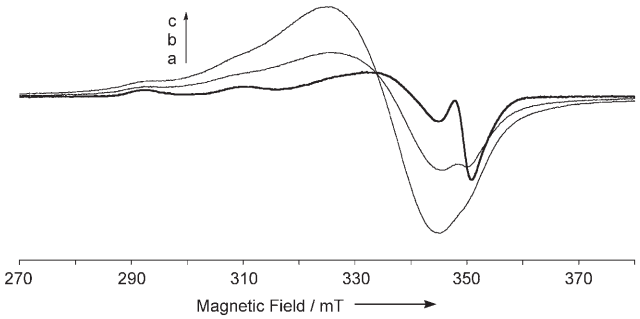


Figure 3. EPR spectra for the copper–cyclam xerogel $\mathbf{X_B}$-**Cu** recorded at 9.79 GHz and 293 K a) before oxygenation, b) after $O_2$ exposure for 3 h, and c) after $O_2$ exposure for 22 h.

valence units is localized to only one copper(II) ion with no delocalization occurring on both copper ions. Before exposure to dioxygen, the EPR spectrum exhibits a four line pattern at room temperature and at 100 K. A nearly axially symmetric signal is observed with a near axial $g$ tensor at $g_{\parallel} = 2.20$ ($A_{\parallel} = 180 \times 10^{-4}\,cm^{-1}$) and $g_{\perp} = 2.05$, characteristic of doublet-spin-state copper(II) ions in a tetragonal geometry. This spectrum is typical of an isolated $Cu^{II}$ ion, which strongly suggests a localized class I mixed-valence $Cu^{I}/Cu^{II}$ structure for the immobilized complexes, as earlier shown by EXAFS spectroscopy. This result is in agreement with a partial self-reduction of $Cu^{II}$ during the pre-treatment procedure. After exposure to $O_2$, the intensities of the EPR spectra increase, but show weak modifications of the tensor parameters ($g_{\parallel} = 2.18$, $g_{\perp} = 2.06$, $A_{\parallel} \approx 180 \times 10^{-4}\,cm^{-1}$); these results indicates that there is no significant alteration of the $Cu^{II}$ ion geometry, that is, only a slight modification of the tetraazamacrocycle ligand field during the oxygenation process occurs. However, because of higher spin interaction coupling between the copper centers, the spectra become featureless and no hyperfine coupling of the unpaired electron with the nuclear spin of the copper ion is observed. This poorly resolved hyperfine structure is due to the high concentration ($1.17\,mmol\,g^{-1}$) of copper ions present in the material that interact with each other through the dioxygen adduct. It was observed that $g_{\parallel} > g_{\perp} > 2.0023$, indicating that the ground-state magnetic orbital containing the unpaired electron corresponds to $d_{x^2-y^2}$; as expected for an axially symmetrical complex in a square-pyramidal or octahedral geometry with a Jahn–Teller axial elongation or a slight equatorial distortion. The main contribution to the EPR linewidth results from dipolar interactions, which broaden the signal; this contribution dominates the magnetic-exchange interactions known to induce narrowing of the signals. The spectrum also contains a weak half-field feature that is assumed to be diagnostic for an exchange-coupled system, leading to a triplet spin state with a weak zero-field splitting. Moreover, there is no disparity between the EPR spectra at 293 and 100 K, which indicates that the copper ions are not mobile, but are strongly coordinated in the tetraazamacrocyclic cavity.

There are several remarkable characteristics of the $Cu^{I}$ reported in this paper. These are: 1) the simplicity of the synthetic protocol, 2) the fact that the partially reversible uptake of dioxygen occurs at room temperature and 3) the reactivity of the class I mixed-valence species towards dioxygen which provides new insights into metal complex–dioxygen interactions.

Compared to the chemistry of copper(I) complexes in solution, the dioxygen adduct is much better stabilized in the solid state when incorporated into a sol–gel matrix; this is due to the protection of the metal ion by the nanostructured solid. Under these conditions the organic–inorganic environment of the copper complexes behaves like a protein in metalloenzymes, protecting the active sites from various substrates and avoiding the formation of byproducts. The engineering of the metal-ion microenvironment and the ion confinement in the solid is a key step to stabilize the dioxygen adduct at room temperature. The dioxygen adduct in copper metalloproteins,[2,3] such as hemocyanin and tyrosinase, leads to strongly antiferromagnetic coupled homovalent μ-peroxodicopper(II) species. This contrasts with the proposed

  

dioxygen adducts in the xerogels, which are associated with a formally mixed-valence μ-superoxo dicopper intermediate and, upon standing at room temperature for few hours, leads to a more stable end-on μ-peroxo dicopper(II) species through a disproportionation process (Scheme 2). Due to the strong antiferromagnetic coupling between the two $Cu^{II}$ ions mediated by the peroxide bridge, the μ-peroxodicopper(II) species in oxohemocyanin and in the $O_2$ adduct of their biomimetic complexes are EPR silent. For this reason the μ-peroxo species in the xerogel should also be EPR silent so the observed EPR signal after oxygenation is most probably due to a homovalent $Cu^{II}$ dinuclear complex (Scheme 2) resulting from the degradation of the dioxygen adduct at 293 K. The copper hydroxo complex leads to a weaker antiferromagnetic coupling between the adjacent $Cu^{II}$ ions than for μ-peroxodicopper(II) dioxygen adducts and it is quite evident than the EPR signal increases during exposure to $O_2$. The side reaction leading to the hydroxo complex is induced by traces of water in the solid, or water generated by the polycondensation reaction of the xerogel, which occurs continuously due to the thermodynamic instability of the solids obtained through the sol–gel process.[25]

In solution, few dinuclear mixed-valence $Cu_2^{I,II}$ complexes are able to react reversibly with dioxygen and the formation of a formally μ-superoxo-dicopper(II) was proposed on the basis of UV/Vis and EPR data.[98] However, with few exceptions, μ-superoxo- and μ-peroxo-dicopper(II) complexes are stable in solution for reasonable periods (hours) only at low temperature ($< -50\,°C$); warming causes decomposition, typically to $Cu^{II}$ complexes through processes involving intramolecular ligand oxidation or dealkylation.[9,99]

The exceptional reactivity of the currently described material shows that the structural organization of the active sites in the silica is regular with a uniform distribution of organic groups within the framework and the cyclam moieties are in close proximity to each other allowing strong interactions between the metal ions. The structural arrangement and periodicity was investigated by XRD measurements: these gave three broad diffraction peaks (Figure 4) and no sharp Bragg reflexion. However, even if the broad signals are too large to be interpreted as a crystalline-like periodicity, they are indicative of a significant organization at the nanometric scale. The low-angle peak ($2\theta = 6.92°$) corresponds to a $d_{100}$ interlayer spacing of 12.7 Å, thus indicating a short-range order.[27,30] This signal can be attributed to the periodic distance of the organic moiety in the largest length, that is, the distance between two N-functionalized propylsiloxanes on the cyclam in a *trans* orientation. In addition, two broad peaks at higher angles corresponding to *d* spacing centered of 4.3 and 8.1 Å are observed. The first peak is always observed for hybrid nanostructured solids[27,100] and is attributable to the alkylated cyclam packing within the layers through the Si–O–Si covalent bonds. Hence, this distance for the molecular scale layered structure represents almost exactly the distance between two adjacent cyclams in the solid. Moreover, it was shown through EXAFS studies (see above) that after complexation of the macrocycles, the intermetallic distances were close to 4 Å. These results show that the molecular scale order remains intact after incorporation of a copper salt into the solid with only a slight modification of the layered nanostructure.

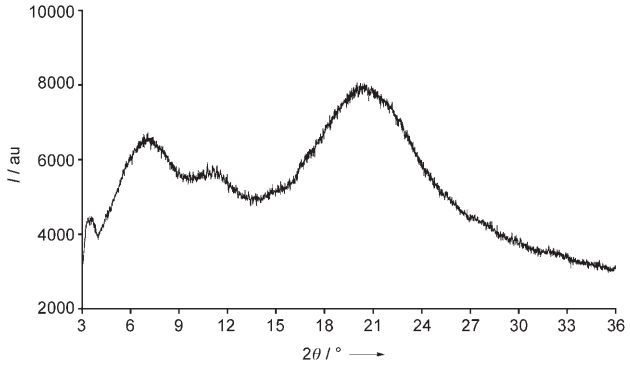


Figure 4. XRD diagram for the copper-free cyclam xerogel $\mathbf{X_B}$ (route B).

As already observed for different organosilica materials,[27,29,30,101–104] the introduction of an organic group into the nanostructure favors anisotropic organization of the molecular units in the amorphous matrix since X-ray scattering exhibits diffraction signals. Indeed, the short-range nano-organization of the tetra-*N*-alkylated cyclam is due to hydrophilic interactions (hydrogen bonds) between silanol functions formed during hydrolysis of the alkoxysilyl functions and van der Waals interactions between hydrophobic chains bearing siloxane groups. This results in a short- to medium-range order.[27,29,30,101–104] This molecular order shows that macrocyclic,[105] rigid[106,107] and flexible organosilylated precursors[30,103,108] are able to induce self-organization of the solid.

The organic distribution observed is in agreement with an anisotropic packing of the tetraazamacrocycle into a regular lamellar structure (Figure 5) with a uniform distribution of the organic units within the framework; thus the cyclam moieties are in close proximity allowing strong interactions between the metal ions. Furthermore, the presence of cyclam N-functionalized by propyl groups provides some flexibility, which should facilitate the oxygenation process by fine tuning of the metal–metal distance during complexation and activation, leading to the reduction of $Cu^{II}$ to $Cu^{I}$. The combination of a quite rigid macrocyclic unit with four flexible hydrophobic alkyl moieties allows increasing interactions between the N-functionalized units during the gelation process due to aggregation forces driven by van der

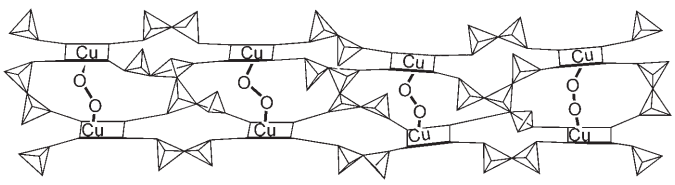


Figure 5. Schematic view of the $O_2$ adduct $\mathbf{X_B}$-**Cu** self-organized in a lamellar polysilsesquioxane structure.

  

Waals interactions. The nanostructuration of the solid explains the activity of the copper ions towards dioxygen coordination at room temperature: almost 100% of the copper ions in the xerogel are active towards dioxygen to form μ-peroxo complexes and partial desorption occurs during heating under vacuum. This result implies, at least, an organization in short range and the rather important flexibility of the ligand in the solid, since the metal–metal distance is able to be fine-tuned during the oxygenation process. The immobilization of the flexible tetraazamacrocycle allows unusual metal coordination stereochemistries, coordination numbers, and oxidation states, leading to the unexpected reactivity of the cyclam copper complexes. This reactivity is thus directly induced by the sol–gel process, which constrains a specific geometry of the macrocycles and ensures their close proximity in a face-to-face configuration before complexation.

However, for the gelated complexes $\mathbf{X_A}$**-Cu** obtained through route A, the rigid type I configuration[63–65] of the complex induces steric constraints between complexes during the gelation, as well as electrostatic repulsions between copper ions, which move away from each other. These constraints avoid the self-reduction of $Cu^{II}$ in a dimeric species, and lead to the expected stable $Cu^{II}$ (showing no reactivity towards $O_2$). The results for $\mathbf{X_A}$**-Cu** and $\mathbf{X_B}$**-Cu** suggest that the coordination chemistry in the solid state and the reactivity of the immobilized species are not directly applicable to the solution studies of the complexes, because the solid organization at short range leads to the confinement of the metallic species.

## Conclusion

The copper cyclams incorporated in the xerogel matrix exhibit an unprecedented affinity for dioxygen binding and the stability of the dioxygen adduct at room temperature is directly related to the nanostructuration of the hybrid material and to the confinement of the copper cyclam complexes. The incorporation of a $Cu^{II}$ center into the material after xerogel formation leads, after an activation step, to a bridged $Cu^{I}/Cu^{II}$ mixed valence dinuclear species. Therefore, the remarkable properties of these copper complexes for $O_2$ adsorption in the silica matrix is induced by the close proximity of the copper ions. This results in end-on $\mu$-$\eta^1$:$\eta^1$-peroxodicopper(II) complexes, and the tetraazamacrocyclic complexes are anisotropically packed in a lamellar structure. We have shown for the first time that the organic–inorganic environment of copper complexes in a silica matrix can fully model the protecting role of proteins for metalloenzymes since an oxygenated dicopper(II) complex can be isolated in a stable form at room temperature and $Cu^{I}$ species can be regenerated after several adsorption–desorption cycles. The coordination scheme and reactivity of the copper cyclams within the solid are totally different to that generally observed in solution. However, the copper xerogels show a lower activity during the adsorption–desorption cycles due to partial decomposition of the active species. This observation prompted us to study a novel class of organic–inorganic nanocomposites named "periodic mesoporous organosilicas" (PMOs).[109–111] In PMOs, the organic groups are located within the channel walls of bridged polysilsesquioxanes. These materials were prepared by a sol–gel process in the presence of a surfactant, which acts as a structuring agent. They exhibit remarkable regularity of the structure with homogeneous repartition of the organic moieties in the framework, high texture stability, and finely tuned pore diameters. The increased stability of the PMOs and the uniformity of the organic dispersion in the inorganic framework compared to xerogels were of great interest in order to obtain stable sorbents of dioxygen. Subsequently, tetra-*N*-[3-tris(alkoxysilyl)propyl]cyclam was incorporated in the PMOs by using a non-ionic triblock copolymer surfactant (Pluronic 123), and their copper complexes were examined for gas separation. After metalation with $CuCl_2$ under argon and thermal activation at 120°C, the material is able to coordinate dioxygen leading to a more stable dioxygen adduct than that observed for the oxygenated complexes in xerogels prepared under nonstructuring conditions. The highest adsorption of dioxygen is obtained when the nonmetalated materials are prepared at 90°C in acidic conditions. The flexible structure of the peripheral *N*-alkyl chains are required to tune the metal–metal distance to a value suitable for the formation of dinuclear $O_2$ adducts. The quantitative metalation reaction of the incorporated ligands inside the framework and the high reactivity of the complex towards dioxygen give further evidence for the high accessibility of the immobilized macrocycles to metallic cations and gases. Moreover, the PMOs incorporating the copper cyclams show a remarkable stability of the $O_2$ adducts, since dioxygen adsorption remains the same after several adsorption–desorption cycles. Study of these materials is still in progress.

## Experimental Section

**General remarks**: The complexation of the xerogels was carried out in a dry argon atmosphere by using a glove box containing less than 3 ppm $O_2$. All solvents were dried carefully and distilled before use. Ethanol was dried on 4 Å molecular sieves and thoroughly degassed under vacuum before transferring to the glove box. Other reagents were of analytical grade, obtained from commercial suppliers and used without further purification. The characterization of the copper(II) precursor complexes was performed in dichloromethane on a UV/Vis Varian Cary 50 spectrophotometer and by mass spectrometry on a BRUKER ProFLEX III spectrometer (MALDI/TOF) using dithranol as the matrix. The copper-complexed materials were characterized using solid state UV/Vis spectra recording in the diffuse reflectance mode on a VARIAN Cary 500 equipped with a Spectralon integration sphere, DRA-CA-50 (LABSPHERE). Powder samples (100 mg) were ground and dispersed in a silica matrix (200 mg, Kieselgel MERCK). The baseline spectrum was obtained from pure silica gel. IR spectral measurements were performed on a BRUKER FT-IR IFS 66v, equipped with a P/N 19900 accessory (GRASEBY SPECAC), in the diffuse reflectance mode. Solid samples were dispersed in KBr. EPR measurements were recorded on a Bruker ESP 300 at X-band (9.7 GHz), equipped with a double cavity and a liquid nitrogen cooling accessory. The spectrum of **1-Cu** was recorded at 100 K in

  

a $CH_2Cl_2$/toluene 3/1 (v/v) mixture ($\approx$5 mmol $L^{-1}$), and at 293 K for the xerogels analyses in the solid state. Xerogels sensitive to dioxygen were transferred in the EPR tube using a glove box under argon. The EPR spectra were referenced to 2,2-diphenyl-1-picrylhydrazyl (DPPH) ($g\sim$ 2.0036). All spectra were recorded by using 100 kHz modulation frequency and microwave power of 20 mW. The characterization was also carried out by using C, H, N microanalyses performed on a FISONS EA 1108 CHNS, while Cu and Si microanalyses were obtained from the "Service Central d'Analyse du CNRS, Lyon". Copper concentration in the xerogel was also analyzed by X-ray fluorescence measurements performed on an Oxford Lab-X 3000. Powder X-ray diffraction experiments were carried out on an INEL CPS-120 diffractometer with a curved counter by using $Cu_{K\alpha}$ radiation. Specific surface areas were measured by $N_2$ adsorption measurements performed at 77 K by using the Brunauer–Emmet–Teller method[112] (BET) on a MICROMERITICS ASAP 2010 analyzer (relative pressure, $P/P_0$, range: 0.05 to 0.25). The cross-sectional area of a nitrogen molecule was assumed to be 0.162 $nm^2$. Average pore diameters were calculated by using Barrett–Joyner–Halenda analysis[113] (BJH). Each sample was previously degassed by heating at 120 °C under vacuum ($10^{-3}$ Torr). $N_2$, $O_2$, and CO adsorption experiments at 293 K were performed by using the same instrument with 60 s equilibration delay. The equilibrium constants for the gas binding affinity, $K_i$, and the adsorption capacity, $V_i$, were calculated by considering two different adsorption processes: selective chemisorption on the copper ion and nonselective physisorption resulting from low-energy adsorption and diffusion of the gas into the solid.[52,74] The experimental data corresponding to the $O_2$ and CO adsorption isotherms were thus analyzed using a model based on two Langmuir-type isotherms [Eq. (1)] and those for $N_2$ with a single Langmuir-type isotherm model [Eq. (2)] with $i = O_2$ or CO.

$$V_i = \frac{V_1 K_1 P}{1 + K_1 P} + \frac{V_2 K_2 P}{1 + K_2 P} \quad (1)$$

$$V_{N_2} = \frac{V_1 K_1 P}{1 + K_1 P} \quad (2)$$

The 1,4,8,11-tetrakis-[3-(triethoxysilyl)-propyl]-1,4,8,11-tetraazacyclotetradecane precursor (**1**) and the mesoporous xerogel ($\mathbf{X_B}$) were prepared as previously reported.[33,114]

**[Cu(1)Cl]Cl (1-Cu)**:[33] Anhydrous $CuCl_2$ (255 mg, 1.9 mmol) was added to a solution of **1** (2 g, 1.96 mmol) in dried ethanol (20 mL) under argon. The reaction mixture was heated (70 °C for 2 h), then the solution was evaporated to dryness. The oily residue was washed twice with pentane (10 mL). The product was obtained as a green oil and dried under vacuum to yield 1.58 g (70 %) of **1-Cu**. MS (MALDI/TOF): $m/z$: 1081.59 $[M-2Cl]^+$, 1018.02 $[M+H-CuCl_2]^+$; UV/Vis ($CH_2Cl_2$): $\lambda_{max}$ ($\varepsilon$) = 806 nm (d–d transition, 199.5 $mol^{-1} dm^3 cm^{-1}$); EPR data ($CH_2Cl_2$/toluene 3:1, 100 K): $g_{\parallel} = 2.24$, $g_{\perp} = 2.06$, $A_{\parallel} = 152 \times 10^{-4}$ $cm^{-1}$; elemental analysis calculated (%) for $C_{46}H_{104}N_4O_{12}Si_4CuCl_2$ (1152.15): C 47.95, H 9.09, N 4.86; found: C 46.89, H 9.29, N 5.24.

**Xerogel $X_A$-Cu**: **1-Cu** (1.37 g, 1.19 mmol) was dissolved in dry ethanol (1.5 mL). After stirring for 5 min at RT, a stoichiometric amount of water (0.13 mL) and a catalytic amount of a molar solution of TBAF (tetrabutylammonium fluoride) in THF (1 %/Si, 12 μL) were added simultaneously to ensure the hydrolytic polycondensation reaction. The solution was stirred for 1 min, then the dark green solution was left at 25 °C and a gel formed after 45 min. The gel was allowed to age at 25 °C for five days before it was ground, filtered, and washed with ethanol and then pentane. The purple solid was then dried under vacuum to yield 900 mg (100 %) $\mathbf{X_A}$**-Cu**. $S_{BET} < 2$ $m^2 g^{-1}$; UV/Vis (diffuse reflectance): $\lambda_{max} = 550$ nm (d–d transition); IR (KBr): 3255 ($\nu$ OH-bonded), 2954 ($\nu_{as}$ C–H), 2854 ($\nu_s$ C–H), 1635 ($\delta$ $H_2O$), 1466 ($\delta$ $CH_2$), 1078 ($\nu$ Si-O-Si), 791 $cm^{-1}$ ($\delta$ Si–OH); [Cu] determined by X-ray fluorescence = 0.94 mmol $g^{-1}$; elemental analysis calculated (%) for $C_{22}H_{44}N_4O_6Si_4CuCl_2 \cdot 9H_2O$ (869.54): C 30.38, H 7.18, N 6.44, Si 12.91, Cu 7.31; found: C 30.04, H 6.51, N 6.24, Si 14.25, Cu 8.10.

**Xerogel $X_B$-Cu**: In a glove box, $\mathbf{X_B}$ (300 mg, $\approx$0.52 mmol) was suspended in thoroughly dried and degassed ethanol (6 mL), then an ethanolic solution (5 mL) of $CuCl_2$ (70.5 mg, 0.52 mmol) was added while stirring. The mixture was heated (70 °C, 12 h), after which the material was filtered, washed three times with ethanol (3 × 5 mL) and dried under vacuum. The drying and activation of the material was done by heating (120 °C, 3 h, $10^{-3}$ Torr) to yield $\mathbf{X_B}$**-Cu** as a clear brown solid (365 mg, 98 %). $S_{BET}$ = 356 $m^2 g^{-1}$; $D_p$ = 10–60 Å; UV/Vis (diffuse reflectance): $\lambda_{max}$ = 740 nm (d–d transition); IR (KBr): 3251 ($\nu$ OH-bonded), 2955 ($\nu_{as}$ C–H), 2752 ($\nu_s$ C–H), 1633 ($\delta$ $H_2O$), 1469 ($\delta$ $CH_2$), 1078 ($\nu$ Si-O-Si), 806 $cm^{-1}$ ($\delta$ Si–OH); [Cu] determined by X-ray fluorescence = 1.17 mmol $g^{-1}$; elemental analysis calculated (%) for $C_{22}H_{44}N_4O_6Si_4CuCl_2 \cdot 5H_2O$ (797.48): C 33.13, H 6.82, N 7.03, Si 14.09, Cu 7.97; found: C 33.19, H 5.45, N 6.73, Si 14.00, Cu 8.00.

[1] J. P. Klinman, *Chem. Rev.* **1996**, *96*, 2541–2562.
[2] E. I. Solomon, U. M. Sundaram, T. E. Machonkin, *Chem. Rev.* **1996**, *96*, 2563–2605.
[3] E. I. Solomon, P. Chen, M. Metz, S.-K. Lee, A. E. Palmer, *Angew. Chem.* **2001**, *113*, 4702–4724; *Angew. Chem. Int. Ed.* **2001**, *40*, 4571–4590.
[4] A. G. Blackman, W. B. Tolman, *Struct. Bonding (Berlin)* **2000**, *97*, 179–211.
[5] M. J. Henson, M. A. Vance, C. X. Zhang, H.-C. Liang, K. D. Karlin, E. I. Solomon, *J. Am. Chem. Soc.* **2003**, *125*, 5186–5192.
[6] L. M. Mirica, X. Ottenwaelder, D. Stack, *Chem. Rev.* **2004**, *104*, 1013–1045.
[7] M. Weitzer, S. Schindler, G. Brehm, S. Schneider, E. Hörmann, B. Jung, S. Kaderli, A. D. Zuberbühler, *Inorg. Chem.* **2003**, *42*, 1800–1806.
[8] C. X. Zhang, S. Kaderli, M. Costas, E. Kim, Y.-M. Neuhold, K. D. Karlin, A. D. Zuberbühler, *Inorg. Chem.* **2003**, *42*, 1807–1824.
[9] E. A. Lewis, W. B. Tolman, *Chem. Rev.* **2004**, *104*, 1047–1076.
[10] S. Schindler, *Eur. J. Inorg. Chem.* **2000**, 2311–2326.
[11] K. A. Magnus, H. Ton-That, J. E. Carpenter, *Chem. Rev.* **1994**, *94*, 727–735.
[12] M. Metz, E. I. Solomon, *J. Am. Chem. Soc.* **2001**, *123*, 4938–4950.
[13] E. J. Land, C. A. Ramsden, P. A. Riley, *Acc. Chem. Res.* **2003**, *36*, 300–308.
[14] J. W. Whittaker, *Chem. Rev.* **2003**, *103*, 2347–2364.
[15] P. Gamez, P. G. Aubel, W. L. Driessen, J. Reedijk, *Chem. Soc. Rev.* **2001**, *30*, 376–385.
[16] S. Itoh, S. Fukuzumi, *Bull. Chem. Soc. Jpn.* **2002**, *75*, 2081–2095.
[17] N. Wei, N. N. Murthy, Q. Chen, J. Zubieta, K. D. Karlin, *Inorg. Chem.* **1994**, *33*, 1953–1965.
[18] M. Harata, K. Jitsukawa, H. Masuda, H. Einaga, *Bull. Chem. Soc. Jpn.* **1998**, *71*, 637–645.
[19] M. Kodera, K. Katayama, Y. Tachi, K. Kano, S. Hirota, S. Fujinami, M. Suzuki, *J. Am. Chem. Soc.* **1999**, *121*, 11006–11007.
[20] Z. Hu, R. D. William, D. Tran, T. G. Spiro, S. M. Gorun, *J. Am. Chem. Soc.* **2000**, *122*, 3556–3557.
[21] M. Kodera, Y. Kajita, Y. Tachi, K. Katayama, K. Kano, S. Hirota, S. Fujinami, M. Suzuki, *Angew. Chem.* **2004**, *116*, 338–341; *Angew. Chem. Int. Ed.* **2004**, *43*, 334–337.
[22] M. Schatz, V. Raab, S. P. Foxon, G. Brehm, S. Schneider, M. Reiher, M. C. Holthausen, J. Sundermeyer, S. Schindler, *Angew. Chem.* **2004**, *116*, 4460–4464; *Angew. Chem. Int. Ed.* **2004**, *43*, 4360–4363.
[23] R. J. P. Corriu, *Eur. J. Inorg. Chem.* **2001**, 1109–1121.
[24] B. Boury, R. J. P. Corriu, *Chem. Commun.* **2002**, 795–802.
[25] G. Cerveau, R. J. P. Corriu, E. Framery, *Chem. Mater.* **2001**, *13*, 3373–3388.
[26] K. J. Shea, D. A. Loy, *Chem. Mater.* **2001**, *13*, 3306–3319.
[27] B. Boury, R. J. P. Corriu, *Chem. Rec.* **2003**, *3*, 120–132.
[28] J. J. E. Moreau, L. Vellutini, M. W. Chi Man, C. Bied, J.-L. Bantignies, P. Dieudonné, J.-L. Sauvajol, *J. Am. Chem. Soc.* **2001**, *123*, 7957–7958.
[29] Y. Kaneko, N. Iyi, K. Kurashima, T. Matsumoto, T. Fujita, K. Kitamura, *Chem. Mater.* **2004**, *16*, 3417–3423.

  

[30] J. J. E. Moreau, L. Vellutini, M. W. Chi Man, C. Bied, P. Dieudonné, J.-L. Bantignies, J.-L. Sauvajol, *Chem. Eur. J.* **2005**, *11*, 1527–1537.
[31] A. Shimojima, Z. Liu, T. Ohsuna, O. Terasaki, K. Kuroda, *J. Am. Chem. Soc.* **2005**, *127*, 14108–14116.
[32] A. M. Kłonkowski, B. Grobelna, T. Widernik, A. Jankowska-Frydel, W. Mozgawa, *Langmuir* **1999**, *15*, 5814–5819.
[33] G. Dubois, R. J. P. Corriu, C. Reyé, S. Brandès, F. Denat, R. Guilard, *Chem. Commun.* **1999**, 2283–2284.
[34] G. Dubois, C. Reyé, R. J. P. Corriu, S. Brandès, F. Denat, R. Guilard, *Angew. Chem.* **2001**, *113*, 1121–1124; *Angew. Chem. Int. Ed.* **2001**, *40*, 1087–1090.
[35] F. Embert, A. Mehdi, C. Reyé, R. J. P. Corriu, *Chem. Mater.* **2001**, *13*, 4542–4549.
[36] S. Bourg, J.-C. Broudic, O. Conocar, J. J. E. Moreau, D. Meyer, M. W. Chi Man, *Chem. Mater.* **2001**, *13*, 491–499.
[37] R. J. P. Corriu, F. Embert, Y. Guari, C. Reyé, R. Guilard, *Chem. Eur. J.* **2002**, *8*, 5732–5741.
[38] M. G. Basallote, E. Blanco, M. Blázquez, M. J. Fernández-Trujillo, R. Litrán, M. A. Máñez, M. R. del Solar, *Chem. Mater.* **2003**, *15*, 2025–2032.
[39] R. J. P. Corriu, E. Lancelle-Beltran, A. Mehdi, C. Reyé, S. Brandès, R. Guilard, *Chem. Mater.* **2003**, *15*, 3152–3160.
[40] J.-M. Barbe, G. Canard, S. Brandès, R. Guilard, *Angew. Chem.* **2005**, *117*, 3163–3166; *Angew. Chem. Int. Ed.* **2005**, *44*, 3103–3106.
[41] T. Kishida, N. Fujita, K. Sada, S. Shinkai, *Langmuir* **2005**, *21*, 9432–9439.
[42] Z.-L. Lu, E. Lindner, H. A. Mayer, *Chem. Rev.* **2002**, *102*, 3543–3578.
[43] H. J. Im, Y. Yang, L. R. Alain, C. E. Barnes, S. Dai, Z. Xue, *Environ. Sci. Technol.* **2000**, *34*, 2209–2214.
[44] M. C. Burleigh, S. Dai, E. W. Hagaman, J. S. Lin, *Chem. Mater.* **2001**, *13*, 2537–2546.
[45] R. D. Makote, S. Dai, *Anal. Chim. Acta* **2001**, *435*, 169–175.
[46] A. G. S. Prado, L. N. H. Arakaki, C. Airoldi, *J. Chem. Soc. Dalton Trans.* **2001**, 2206–2209.
[47] A. Walcarius, C. Delacote, S. Sayen, *Electrochim. Acta* **2004**, *49*, 3775–3783.
[48] Y.-K. Lu, X.-P. Yan, *Anal. Chem.* **2004**, *76*, 453–457.
[49] M. Tsionsky, O. Lev, *Anal. Chem.* **1995**, *67*, 2409–2414.
[50] S. Blair, R. Kataky, D. Parker, *New J. Chem.* **2002**, *26*, 530–535.
[51] C. Sanchez, B. Lebeau, F. Chaput, J.-P. Boilot, *Adv. Mater.* **2003**, *15*, 1969–1994.
[52] G. Dubois, R. Tripier, S. Brandès, F. Denat, R. Guilard, *J. Mater. Chem.* **2002**, *12*, 2255–2261.
[53] J. Goulon, C. Goulon-Ginet, A. Rogalev, F. Wilhelm, N. Jaouen, D. Cabaret, Y. Joly, G. Dubois, R. J. P. Corriu, G. David, S. Brandès, R. Guilard, *Eur. J. Inorg. Chem.* **2005**, 2714–2726.
[54] C. Malins, S. Fanni, H. G. Glever, J. G. Vos, B. D. MacCraith, *Anal. Commun.* **1999**, *36*, 3–4.
[55] D. Parker, *Coord. Chem. Rev.* **2000**, *205*, 109–130.
[56] E. S. Ribeiro, Y. Gushikem, J. C. Biazzotto, O. S. Serra, *J. Porphyrins Phthalocyanines* **2002**, *8*, 527–532.
[57] H. Zhang, Y. Sun, K. Ye, P. Zhang, Y. Wang, *J. Mater. Chem.* **2005**, *15*, 3181–3186.
[58] Y. Wang, X. Jiang, Y. Xia, *J. Am. Chem. Soc.* **2003**, *125*, 16176–16177.
[59] M. Meyer, V. Dahaoui-Gindrey, C. Lecomte, R. Guilard, *Coord. Chem. Rev.* **1998**, *178–180*, 1313–1405.
[60] Y. Dong, G. A. Lawrance, L. F. Lindoy, P. Turner, *Dalton Trans.* **2003**, 1567–1576.
[61] T. J. Hubin, *Coord. Chem. Rev.* **2003**, *241*, 27–46.
[62] F. Denat, S. Brandès, R. Guilard, *Synlett* **2000**, 561–574.
[63] A. E. Goeta, J. A. K. Howard, D. Maffeo, H. Puschmann, J. A. G. Williams, D. S. Yufit, *J. Chem. Soc. Dalton Trans.* **2000**, 1873–1880.
[64] C. Bucher, E. Duval, J.-M. Barbe, J.-N. Verpeaux, C. Amatore, R. Guilard, *C. R. Acad. Sci. Paris, Ser. IIc* **2000**, *3*, 211–222.
[65] P. Comba, P. Jurisic, Y. D. Lampeka, A. Peters, A. I. Prikhod'ko, H. Pritskow, *Inorg. Chim. Acta* **2001**, *324*, 99–107.
[66] L. Siegfried, A. Comparone, M. Neuburger, T. A. Kaden, *Dalton Trans.* **2005**, 30–36.
[67] X. Liang, P. J. Sadler, *Chem. Soc. Rev.* **2004**, *33*, 246–266.
[68] D. Parker, *Chem. Soc. Rev.* **2004**, *33*, 156–165.
[69] F. Cuenot, M. Meyer, E. Espinosa, R. Guilard, *Inorg. Chem.* **2005**, *44*, 7895–7910.
[70] M. Mägi, E. Lippmaa, A. Samoson, G. Engelhardt, A.-R. Grimmer, *J. Phys. Chem.* **1984**, *88*, 1518–1522.
[71] R. S. Drago, C. E. Webster, J. M. McGilvray, *J. Am. Chem. Soc.* **1998**, *120*, 538–547.
[72] C. E. Webster, A. Cottone III, R. S. Drago, *J. Am. Chem. Soc.* **1999**, *121*, 12127–12139.
[73] C. E. Webster, R. S. Drago, *Microporous Mesoporous Mater.* **1999**, *33*, 291–306.
[74] J.-M. Barbe, G. Canard, S. Brandès, F. Jerome, G. Dubois, R. Guilard, *Dalton Trans.* **2004**, 1208–1214.
[75] L. Que Jr, W. B. Tolman, *Angew. Chem.* **2002**, *114*, 1160–1185; *Angew. Chem. Int. Ed.* **2002**, *41*, 1114–1137.
[76] Y. Tachi, K. Aita, S. Teramae, F. Tani, Y. Naruta, S. Fukuzumi, S. Itoh, *Inorg. Chem.* **2004**, *43*, 4558–4560.
[77] K. Komiyama, H. Furutachi, S. Nagatomo, A. Hashimoto, H. Hayashi, S. Fujinami, M. Suzuki, T. Kitagawa, *Bull. Chem. Soc. Jpn.* **2004**, *77*, 59–72.
[78] R. R. Jacobson, Z. Tyeklar, A. Farooq, K. D. Karlin, S. Liu, J. Zubieta, *J. Am. Chem. Soc.* **1988**, *110*, 3690–3692.
[79] A. Wada, Y. Honda, S. Yamaguchi, S. Nagatomo, T. Kitagawa, K. Jitsukawa, H. Masuda, *Inorg. Chem.* **2004**, *43*, 5725–5735.
[80] S. R. Breeze, S. Wang, *Inorg. Chem.* **1996**, *35*, 3404–3408.
[81] D. D. LeCloux, R. Davydov, S. J. Lippard, *Inorg. Chem.* **1998**, *37*, 6814–6826.
[82] J. Kuzelka, S. Mukhopadhyay, B. Spingler, S. J. Lippard, *Inorg. Chem.* **2004**, *43*, 1751–1761.
[83] P. Comba, M. Zimmer, *Inorg. Chem.* **1994**, *33*, 5368–5369.
[84] B. Bosnich, C. K. Poon, M. L. Tobe, *Inorg. Chem.* **1965**, *4*, 1102–1108.
[85] H. Aneetha, Y.-H. Lai, S.-C. Lin, K. Panneerselvam, T.-H. Lu, C.-S. Chung, *J. Chem. Soc. Dalton Trans.* **1999**, 2885–2892.
[86] C. Bucher, E. Duval, E. Espinosa, J.-M. Barbe, J.-N. Verpeaux, C. Amatore, R. Guilard, *Eur. J. Inorg. Chem.* **2001**, 1077–1079.
[87] J. Chapman, G. Ferguson, J. F. Gallagher, M. C. Jennings, D. Parker, *J. Chem. Soc. Dalton Trans.* **1992**, *109*, 345–353.
[88] M. R. Oberholzer, M. Neuburger, M. Zehnder, T. A. Kaden, *Helv. Chim. Acta* **1995**, *78*, 505–513.
[89] E. V. Rybak-Akimova, A. Y. Nazarenko, L. Chen, P. W. Krieger, A. M. Herrera, V. V. Tarasov, P. D. Robinson, *Inorg. Chim. Acta* **2001**, *324*, 1–15.
[90] G. A. McLachlan, G. D. Fallon, R. L. Martin, L. Spiccia, *Inorg. Chem.* **1995**, *34*, 254–261.
[91] T. H. Bennur, D. Srinivas, S. Sivasanker, *J. Mol. Catal. A* **2004**, *207*, 163–171.
[92] T.-J. Lee, T.-Y. Lee, C.-Y. Hong, D.-T. Wu, C.-S. Chung, *Acta Crystallogr. Sect. C* **1986**, *42*, 999–1001.
[93] H. Kurosaki, C. Bucher, E. Espinosa, J.-M. Barbe, R. Guilard, *Inorg. Chim. Acta* **2001**, *322*, 145–149.
[94] S. C. Larsen, A. Aylor, A. T. Bell, J. A. Reimer, *J. Phys. Chem.* **1994**, *98*, 11533–11540.
[95] S. Recchia, C. Dossi, R. Psaro, A. Fusi, R. Ugo, G. Moretti, *J. Phys. Chem. B* **2002**, *106*, 13326–13332.
[96] M. H. Groothaert, J. A. van Bokhoven, A. A. Battiston, B. M. Weckhuysen, R. A. Schoonheydt, *J. Am. Chem. Soc.* **2003**, *125*, 7629–7640.
[97] G. T. Palomino, P. Fisicaro, S. Bordiga, A. Zecchina, E. Giamello, C. Lamberti, *J. Phys. Chem. B* **2000**, *104*, 4064–4073.
[98] M. Mahroof-Tahir, K. D. Karlin, *J. Am. Chem. Soc.* **1992**, *114*, 7599–7601.
[99] S. Teramae, T. Osako, S. Nagatomo, T. Kitagawa, S. Fukuzumi, S. Itoh, *J. Inorg. Biochem.* **2004**, *98*, 746–757.
[100] Y. Kaneko, N. Iyi, T. Matsumoto, K. Fuji, K. Kurashima, T. Fujita, *J. Mater. Chem.* **2003**, *13*, 2058–2060.

  

[101] N. Liu, K. Yu, B. Smarsly, D. R. Dunphy, Y.-B. Jiang, C. J. Brinker, *J. Am. Chem. Soc.* **2002**, *124*, 14540–14541.
[102] G. Cerveau, R. J. P. Corriu, E. Framery, F. Lerouge, *J. Mater. Chem.* **2004**, *14*, 3019–3025.
[103] J. Alauzun, A. Mehdi, C. Reyé, R. J. P. Corriu, *J. Am. Chem. Soc.* **2005**, *127*, 11204–11205.
[104] M. P. Kapoor, S. Inagaki, S. Ikeda, K. Kakiuchi, M. Suda, T. Shimada, *J. Am. Chem. Soc.* **2005**, *127*, 8174–8178.
[105] M. Barboiu, S. Cerneaux, A. van der Lee, G. Vaughan, *J. Am. Chem. Soc.* **2004**, *126*, 3545–3550.
[106] A. Sayari, W. Wang, *J. Am. Chem. Soc.* **2005**, *127*, 12194–12195.
[107] J. J. E. Moreau, B. P. Pichon, M. W. Chi Man, C. Bied, H. Pritzkow, J.-L. Bantignies, P. Dieudonné, J.-L. Sauvajol, *Angew. Chem.* **2004**, *116*, 205–208; *Angew. Chem. Int. Ed.* **2004**, *43*, 203–206.
[108] A. Shimojima, K. Kuroda, *Langmuir* **2002**, *18*, 1144–1149.
[109] T. Asefa, M. J. MacLachlan, N. Coombs, G. A. Ozin, *Nature* **1999**, *402*, 867–871.
[110] S. Inagaki, S. Guan, Y. Fukushima, T. Ohsuna, O. Terasaki, *J. Am. Chem. Soc.* **1999**, *121*, 9611–9614.
[111] B. J. Melde, B. T. Holland, C. F. Blanford, A. Stein, *Chem. Mater.* **1999**, *11*, 3302–3308.
[112] S. Brunauer, P. H. Emmet, E. Teller, *J. Am. Chem. Soc.* **1938**, *60*, 309–319.
[113] E. Barrett, L. G. Joyner, P. P. Halenda, *J. Am. Chem. Soc.* **1951**, *73*, 373–380.
[114] R. J. P. Corriu, A. Mehdi, C. Reyé, C. Thieuleux, *New J. Chem.* **2003**, *27*, 905–908.

Received: August 11, 2006
Published online: January 15, 2007

  